Bull. Mater. Sci., Vol. xx, No. x, Month 2017, pp. xxx–xxx
DOI 10.1007/sxxxx-0xx-1xyz-8

simple solid state method to synthesize nanosize ferromagnetic α-Fe_2O_3 with enhance photocatalytic activity in sunlight

MADHAVI D. SHETE[1*] and JULIO B. FERNANDES[2]
[1,2]Department of Chemistry, Goa University, Taleigao Plateau, Goa. 403206, India
*Author for correspondence (smadhavi91@gmail.com)

MS received

Short Title: *Synthesis of ferromagnetic α-Fe_2O_3 with high photocatalytic activity.*

Abstract. **An α-Fe_2O_3 was synthesized by preparing a mixture of iron (III) nitrate with urea as precursor. The yellowish coloured precursor was calcined at 400 ºC for 2 h, resulting in formation of bright red coloured hematite. The surface properties and catalytic activity were compared with a reference sample prepared without the use of urea. It was observed that the urea induced synthesis resulted in a sample having nanosize and large lattice strain, accompanied by development of ferromagnetic behavior. The catalytic activity was evaluated for decomposition of H_2O_2 through photo-Fenton process in sunlight. The urea synthesized sample showed an usually large photo-Fenton effect and the catalyst could be easily recovered and reused due to its ferromagnetic behavior.**

Keywords. Hematite, ferromagnetism, lattice strain, photo-Fenton process, H_2O_2

1. Introduction

Iron is one of the most abundant elements in the earth's crust. Its oxide exists in different polymorphic forms such as hematite and magnetite. Like various transition metal oxide, iron oxides exhibit different bulk properties such as magnetism and surface properties. Properties of an iron oxide depends on the method of synthesis e.g co-precipitation method is a simple and efficient technique also include good homogeneousness, low cost, low time consumption [1-3].

Among the various iron oxides, the hematite or α-Fe_2O_3 form is a thermodynamically stable oxide. Hematite is an important and widely investigated polymorph of iron oxide. It has hexagonal close packed crystal structure with band gap of 2.1eV. It is known to have a large number of applications in the area of sensors, capacitors and as a catalytic material as well as in energy conversion through photoelectrochemical process. It is particularly relevant as compared to other transition metal oxides due to its ease of synthesis and non toxic nature. Hematite is generally antiferromagnetic however its oxygen deficient form is known to exhibit significant ferromagnetic or superparamagnetic behavior [4]. At temperatures below 948 K bulk hematite is an antiferromagnetic material with slightly canted spins and at 200 K spins flip 90 degrees and the hematite phase becomes pure antiferromagnetic. The phenomenon of magnetism in hematite was explained by Krinchik et al. based on the investigation of natural faces of hematite band calculating the energy of surface anisotropy for the faces of type (100) and (111) in hematite [5]. Weak ferromagnetic moment within the basal plane of hematite natural crystals at low temperatures was explained by Hernandez et al [6].

Apart from the magnetic properties of α-Fe_2O_3, it can be also used as good candidate for use in heterogeneous Fenton like process because they are reactive at neutral pH which avoids the need for the acidification and neutralization steps used in the homogeneous Fenton process.

Also their low band gap and magnetic property helps to undergo facile advance oxidation process and to separate out from the reaction mixture easily [7-12].

In the present study we have synthesized iron oxide by combustion method. Synthesized samples were further investigated for their surface and magnetic properties. The results are also discussed in relation to the catalytic activity towards decomposition of hydrogen peroxide. In the present investigation we report a urea induced synthesis of hematite having ferromagnetic properties.

2. Experimental

2.1 Synthesis of α-Fe_2O_3

All the chemicals used were of analytical grade. Fe $(NO_3)_3.9H_2O$, 99-101 % and urea $CO(NH_2)_2$, 99-100.5 % were purchased from Thomas Baker (Chemicals), Pvt. Ltd. (Mumbai). Iron oxides were synthesized by heating an intimate solid mixture of ferric nitrate ± urea such that the ferric nitrate: urea molar compositions were 1: 0 and 1: 5. The mixtures were preheated uniformly on a water bath. This resulted in the formation of a molten liquid at 60 ^{o} C. Thereafter (within ~ 1 – 2 hours) the mixture became semisolid. When the temperature was raised to ~ 90 ^{o} C, the reaction mixture got converted into a dry powdery mass within ~ 2 hours. The resulting precursors were subsequently heated in a muffle furnace at 400 ^{o} C for 2 h to obtain the final samples (Scheme 1). The samples in general were designated as F-xy where xy is molar ratio of ferric nitrate and urea. Their respective sample codes were F-10 and F-15.

2.2 Characterization

Phase identification was carried out from the X-ray powder diffraction patterns (XRD) recorded on a Rigaku Ultima IV diffractometer, using Ni filtered Cu Kα radiation (λ=1.5406A^{o}). The crystallite sizes were determined using the Scherrer formula $t = 0.9\lambda / \beta\cos\theta$ where λ is the wavelength characteristic of the Cu Kα radiation, β is the full width at half maximum (in radians) and θ is the angle at which the 100 intensity peak appears. Thermal studies were carried out on NETZSCH STA 409 PC by using Al_2O_3 crucible at the heating rate 10^{o}C/min in oxygen atmosphere. TEM analyses were carried out to find the particle size of the synthesized catalyst on Phillips CM 200 operating voltages: 20 – 200 kV resolution: 2.4 A^{o}. The BET surface area was determined by a multipoint BET method and BJH pore size distribution analysis on Quantachrome Autosorb iQ and Asiqwin gas sorption system. The band gap energies were determined using UV-VIS spectrophotometer (Shimadzu UV-2450). FT-IR spectrum was recorded in the 4000 - 400 cm^{-1} on Shimadzu IR Prestige-21 by diluting a few milligrams of sample in KBr. The magnetic properties were measured on Quantachrome Versa Lab vibrating sample magnetometer (VSM) at 300 K. XPS spectra recorded for the representative sample on microtech multiple ESCA 3000 spectrometer.

2.3 Catalytic activity

The catalytic activity was measured by the ability of the catalyst to decompose H_2O_2. The decomposition of H_2O_2 was carried out on 10 mg of the catalyst containing 5 mL of 0.1 M H_2O_2 and measuring the evolved gas at various time intervals. The reactions were carried in dark as well in sunlight. The pH of the reaction mixture was 5.

3. Results and discussion

3.1 Synthesis and characterization

The urea induced synthesis of the iron oxide is illustrated in (Scheme 1). It is known that Fe (III) nitrate when calcined produces the hematite phase. When this calcination is carried out in presence of urea, the surface features of the oxides get altered. In the present investigation, the synthesis was carried by using salt:urea ratio of 1:5, which is close to the stoichiometric ratio required for combustion synthesis [13-14]. Calcination of the precursors was carried out at 400 ^{o}C. XRD patterns for the synthesized samples are as shown in Figure 1. In case of both the samples F-10 and F-15; all the peaks correspond to the hematite or α-Fe_2O_3 phase. These are in agreement with JCPDS, file no. 33-0664. Table 1 gives the synthesis and the structural parameters of the samples. As seen from the TG curves (figure 2), the decomposition of the

iron oxide precursors get completed by 400 °C, resulting in stable phase formation.
Figure 3 gives TEM images for the synthseized samples and their respective paricle sizes are given in (Table 1). The TEM particle sizes were 23 and 37 nm respectively. Thus the urea synthesized sample F-15, showed larger particle size. This could be due to increase in the temperature caused by the use of urea during the synthesis; 'the exothermic effect leading to formation of crystallites of larger size'. The high temperatures during combustion synthesis can cause lattice disorders and cation displacements resulting in strain in the lattice.

Table 1 also gives the values of the lattice strain calculated with reference to Williamson-Hall plots [15] As expected F-15 showed much larger strain (a value of 0.165) as compared to only (0.063) for F-10, the latter was synthesized by calcination of precursor without the use of urea.. Figure 4 gives IR spectra of the synthesized samples. IR vibrations obtained in the region of 400-1000 cm^{-1} were due to the Fe-O bonds [16]. The bands between 1200 – 1800 cm^{-1}.are attributed to solid state defects or lattice imperfections, which generally arise in samples prepared by combustion method. Solid state defects could be oxygen defects and absence of some lattice oxygen around Fe^{3+}. The sample F-10 also showed bands around 3460 and 1636 cm^{-1} due to O-H stretching and bending absorptions. These bands were absent in F-15 as during urea induced synthesis the high temperature causes complete dehydroxylation followed by in situ sintering of some particles. This explains the larger particle size and higher lattice strain in the F-15 sample.

In α-Fe_2O_3, Fe^{3+} is a $3d^5$ complex surrounded by O^{2-} ions in octahedral environment. Fig. 5 gives the UV Vis spectra of the synthesized α-Fe_2O_3 samples F-10 and F-15. The spectra show absorptions at wavelengths around (i) ~ 350 nm, mainly due to ligand to metal charge transfer process (LMCT) (ii) ~ 530 nm in the range 450 – 600 nm, due to transitions associated with magnetically coupled cations which is a pair excitation processes of the type $^6A_1 + {}^6A_1 \rightarrow {}^4T_2$ (4G) + $^4T_2$ (4G) as well as d-d transition associated with high spin Fe^{3+} and (iii) a weak absorption in the spectral range of 600 – 800 nm which is due to ligand field transition of Fe^{3+}.
In F-15, the UV-Vis absorption intensities in the range 200-600 nm, are significantly lower than that of F-10, due to O^{2-} vacancies, causing incomplete coordination around the metal ion, which in turn affect the ligand to metal charge transfer.

Figure 6 gives N_2 adsorption - desorption isotherms with respective pore size distributions (profiles as insets). F-10 and F-15 show hysteresis from 0.3 to 1 relative pressures. The respective surface areas are given in the (Table 1).

There is no much difference observed in case of surface area of the sample F-10 and F-15 but the pore size distribution profiles of F-15 differ from that of F-10. F-15 exhibits different pores of different sizes ranging from 10 - 20 A°, 20 – 30A° and 40 - 60 A°. The observed wide range of porosity in F-15 is due to use of urea during the synthesis process. The large amount of gases evolved during the calcinate stage induce wider porosity range.

3.2 Magnetic properties

Figure 7, gives the magnetization curves and the corresponding hysterisis parameters. The respective magnetic values are given in (Table 2) The sample F-10, synthesized without urea, as expected, shows essentially antiferromagetic behaviour or very weak ferromagnetism due to a small spin canting effect. In fact its room temperature saturation magnetism is very weak (~ 0.8 emu g^{-1}). On the other hand the sample synthesized in presence of urea showed large ferromagnetism (~ 15.4 emu g^{-1}).
As urea mediated synthesis, induces O^{2-} vacancies, it results in incomplete coordination environment of O^{2-} ligands for Fe^{3+}. It thus destroys the antiferromagnetic super-exchange interaction $Fe^{3+} – O^{2-} – Fe^{3+}$, resulting in uncompensated magnetism.
Figure 8 gives the XPS spectra of F-15. The peaks due to 2p3/2 and 2p1/2 were observed at binding energies of 709 eV and 718 eV respectively, and spaced apart with a binding energy difference of 13 eV as observed in α-Fe_2O_3 nanostructures [20,21]. Further, satellite shake-up peaks were observed at the higher binding energy side of the above two main peaks. Thus these peaks were observed at 718 eV and 731eV which were about + 9eV upside in energy and are due to presence of Fe^{3+}. Thus there were no traces of Fe or Fe^{2+} or γ-Fe_2O_3 in the F-15 sample that could have contributed to its ferromagnetic property.

3.3 Catalytic activity for decomposition of H_2O_2.

The catalytic activity of the samples was studied for their ability to decompose H_2O_2. The investigation was carried out by keeping the reaction mixture first in the dark (absence of sunlight) and another mixture in the sunlight. The relative activities were compared at different time intervals and results are summarized in (Table 3). It can be seen from (figure 9) both the samples showed similar reactivity in dark. The slightly higher activity of F-10 may be attributed to its slightly larger surface area available for the adsorption of H_2O_2 prior to its decomposition. The hematite iron oxide known to be active for the decomposition of H_2O_2 via Fenton like process. Fenton reagent is a mixture of $FeSO_4$+H_2O_2 which acts as an oxidizing agent. In the case of this catalyzed reaction the surface ferric ions (Fe^{3+}) interact with H_2O_2 in acidic media by release of Fe^{2+} and thus

generate Fenton reagent Fe^{2+} (H_2O_2) in situ. The general decomposition reaction on iron oxide catalyst can be written as in (equation 1) by taking up Fe^{3+} ions from the catalyst surface. Fe^{2+} thus generated, catalyze further decomposition of H_2O_2 through intermediate formation of HO^{*} and HO_2^{*} [18] While the catalytic activity in dark was similar for both the samples, the urea synthesized sample F-15 showed a large difference in reactivity when the reaction mixture was exposed to sunlight. It can be seen from Table 3 that F-10 showed enhancement in reactivity in sunlight by liberating additional volume (ΔV) of 5 mL of oxygen gas in the sunlight. Under the same condition, F-15 showed additional liberation of 41 mL of oxygen. Thus F-15 was eight times more reactive in the sunlight. Other iron oxides are also being reported with ferric nitrate and urea molar ratio 1:2 and 1:3 to be showing comparatively low catalytic activity than F-15 [19].

Following mechanism is therefore proposed for the observed photo-Fenton process (Scheme: 2)

It is seen earlier that both the samples showed similar band gap (2.1eV). Hence the high photo-Fenton activity of F-15 could not be explained by relative band gap values. It is seen that F-15 has much larger lattice strain indicating presence of large number of solid state defects associated with the presence of oxygen vacancies which cause incomplete coordination environment for Fe^{3+}. This facilitates capture of conduction band electrons at such defect centres and thus enhance the rates of the intermediate reactions as envisaged in Scheme 2 and consequently enhance decomposition of H_2O_2. The high ferromagnetic character of F-15 can help in easy recovery and reuse of the catalyst.

4. Conclusion

(i) A hematite or α–Fe_2O_3 was synthesized by calcination of a Fe(III) nitrate –urea precursor in air at 400 °C. The sample was designated as F-15 to signify 1:5 molar ratio of salt: urea.

(ii) The samples were characterized by XRD for identification of the hematite phase, IR for presence of Fe-O bond and solid state defects. A band gap of around 2.1 was observed from UV-Vis spectroscopic technique.

(iii) The observed TEM particle size of 37 nm was larger for F-15 than the sample F-10 prepared without use of urea.

(iv) F-15 showed ferromagnetic behavior with a saturation magnetism of 15.4 emu/g with a significant remanance of 3.2 emu/g.

(v) It also showed large catalytic activity for decomposition of H_2O_2 , due to photo-Fenton effect, which was at least 8 times larger than the F-10 sample. The F-15 catalyst being ferromagnetic could be easily recovered from the reaction mixture.

Acknowledgements

One of the authors, Madhavi Shete is grateful to UGC-BSR fellowship for providing student fellowship

References

[1] Jing X, Haibin Y, Wuyou F, Kai D, Sui Y, Chen J, Zeng Y, Li M, Zou G 2007 *J. Magn. Magn. Mater.* **309** 744.

[2] Fang B, Wang F, Zhang W, Li M, Kan X 2005 *Electroanalysis* **17** 744.

[3] Gupta A K, Gupta M 2005 *Biomater* **26** 3995.

[4] Boer C, Dekkers M 2001 *Geophys. J. Int* **144** 481

[5] Krinchik G S, Zubov V 1990 *J. Magnetism and Magnetic Mater.* 86 105

[6] Hernandez F 2013 *Geochemistry Geophysics Geosystem* **14** 4444

[7] Pinto I S X, Pacheco P, Coelho J V, Lurencon E, Andisson J, Fabris J, Pereira M 2012 *Appl. Cat. B: Environmental* **119** 175.

[8] Tang L, Tang J, Zang G, Yang G, Xie X, Zhou Y, Pang Y, Fang Y, Wang J, Xiong W 2015 *Appl. Surf. Sci.* **333** 220

[9] Paola A D , Augugliaro V, Palmisano L, Pantaleo G, Savonav E 2003 *J. Photochem. And Photobiol. A: Chem.* **155** 207.

[10] Yu M, Zhao S, Asuha S 2013 *J. Porous Mater.* **20** 1353.

[11] Karunakaran C, Senthilvelan S 2006 *Electrochem. Comm.* **8** 95.

[12] Pradhan G K, Padhi D K, Parida K M 2013 *ACS Appl. Mater. Interfaces*, **5 (18)** 9101.

[13] Zhao S, Wu H Y, Song L, Tegus O 2009 *J. Mater Sci.* **44** 926.

[14] Asuha S, Zhao S, Jin X H, Hai M M, Bao H P 2009 *Appl Surf Sci.* **255** 8897.

[15] Williamson G. K and Hall W H 1953 *Acta. Metall.* **1** 22.

[16] Vempati R K, Loeppert R H, Bhatkar H S1990 *Clays and clay minerals* **38** 294.

[17] Kai H. Lei W X, Hong Y, Wu W W 2011 *Chin, Phys Letts*, **28** 117701

[18] Wang C, Liu H, Sun Z 2012 *Inter. J. Photoenergy*, 1110.

[19] Shete M D, Fernandes J B 2015 *Mat. Chem. Phy.* **165** 113.

[20] Al-Gaashani R, Radiman S, Tabet N, Daud A R, 2015 *J. Alloys and Compounds*, **550** 395

[21] Mirzaeil A, Janghorban K, Hashemi B, Hosseini S, Bonyani M,Leonardi S G, Bonavita A, Neri G 2016 *Processing and Application of Ceramics* **10** 209

Scheme

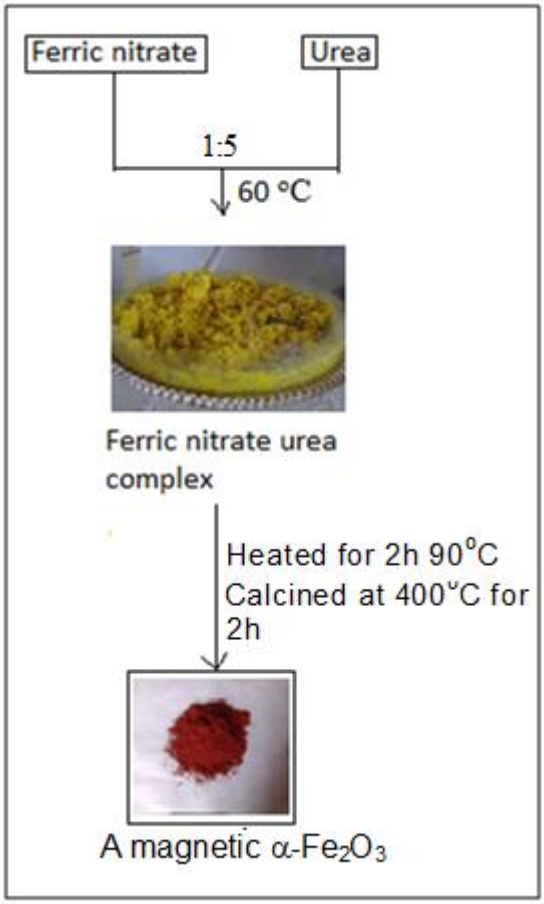

Scheme 1 : Urea induced synthesis of a magnetic α-Fe_2O_3

Equations

$Fe_2O_3(s) + 4H^+ + H_2O_2 \rightarrow 2Fe^{2+} + 3H_2O + O_2$ (1)

$Fe_2O_3(s) + h\upsilon \rightarrow e^-_{CB} + h^+_{VB}$ (a)

$Fe^{3+}_{(s)} + e^-_{CB} \rightarrow Fe^{2+}$ (b)

$Fe^{2+} + H_2O_2 \rightarrow Fe^{3+} + OH^- + HO^*$ (c)

$HO^{*\cdot} + H_2O_2 \rightarrow HO_2^* + H_2O$ (d)

$Fe^{3+} + HO_2^* \rightarrow Fe^{2+} + O_2 + H^+$ (e)

$h^+_{VB} + Fe^{2+} \rightarrow Fe^{3+}$ (f)

Adding together the various steps (a)(b) (c) (d) (e) and (f)

$2H_2O_2 \longrightarrow 2H_2O + O_2$ (2)

Scheme 2: decomposition of H_2O_2 on Fe_2O_3 catalyst in presence of sunlight

Tables

Table 1 Synthesis and structural properties of the α-Fe_2O_3 samples prepared by calcination of iron nitrate ± urea mixture.

Catalyst code	Urea mol	Phase composition	Particle size (nm)	Lattice parameters (A°) a=b	c	c/a	Lattice strain	Surface area (m^2/g)	Pore volume (cc/g)	Pore radius (A°)	Band gap (eV)
F-10	0	α-Fe_2O_3	23	5.03	13.77	2.73	0.063	44	0.185	17.03	2.1
F-15	5	α-Fe_2O_3	37	5.02	13.75	2.73	0.165	43	0.090	21.55	2.1

Table 2 : Magnetic properties of the samples

Catalyst code	Particle size (nm)	Magnetic properties Ms (emu/g)	Mr (emu/g)	Hc (Oe)
F-10	23	0.783	0.103	1978.22
F-15	37	15.431	3.216	271.76

Table 3 Surface area and decomposition of H_2O_2 on the synthesized samples.

Catalyst code	Surface area (m^2/g)	Pore volume (cc/g)	Pore radius (A°)	Volume of O_2 gas (mL) after 50 sec Dark	Sunlight	Enhancement in reactivity in sunlight, ΔV (mL)
F-10	44	0.185	17.033	9.3	14.3	5
F-15	43	0.090	21.550	7.8	49	41.2

Figures

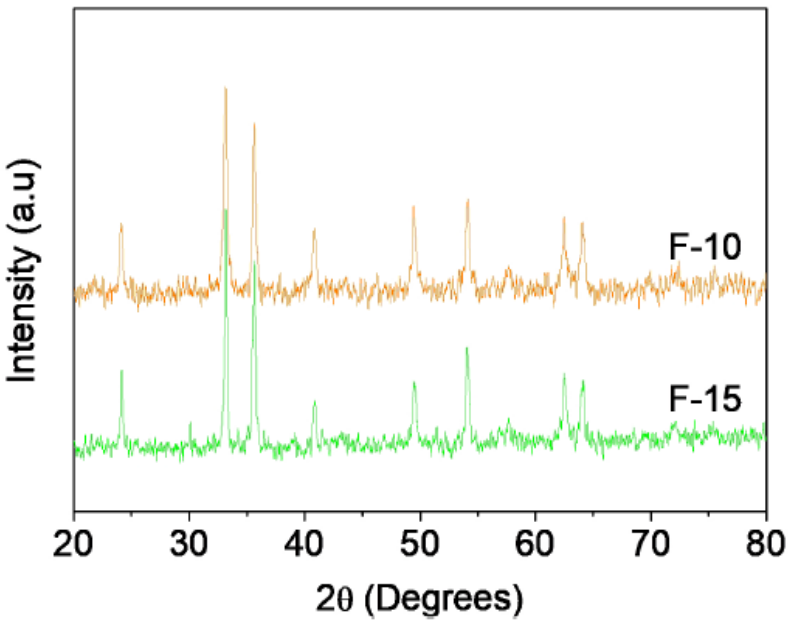

Figure 1. XRD pattern of synthesized samples F-10 and F-15

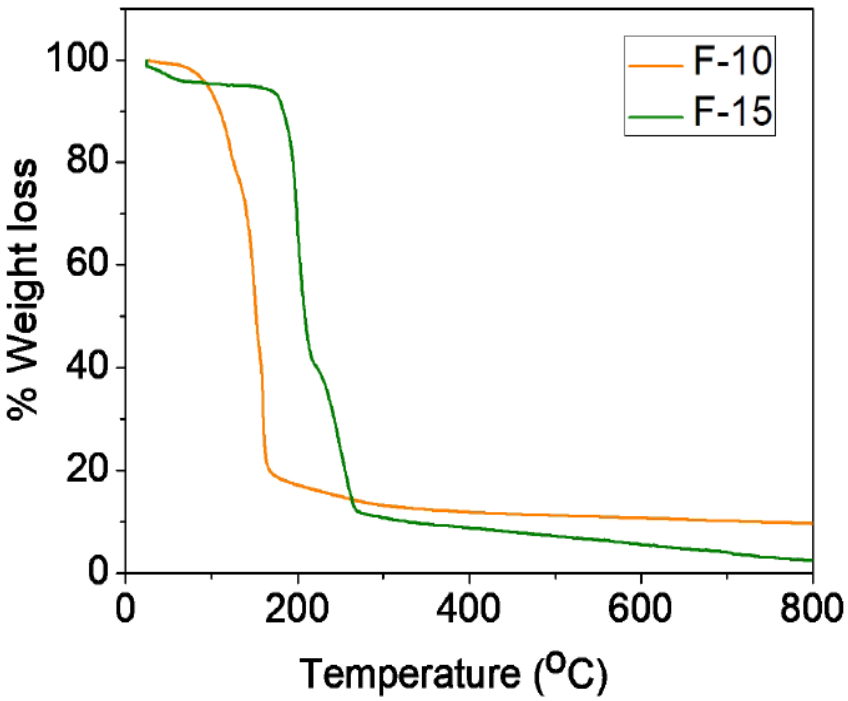

Figure 2. TG curves of the synthesized precursors of sample F-10 and F-15.

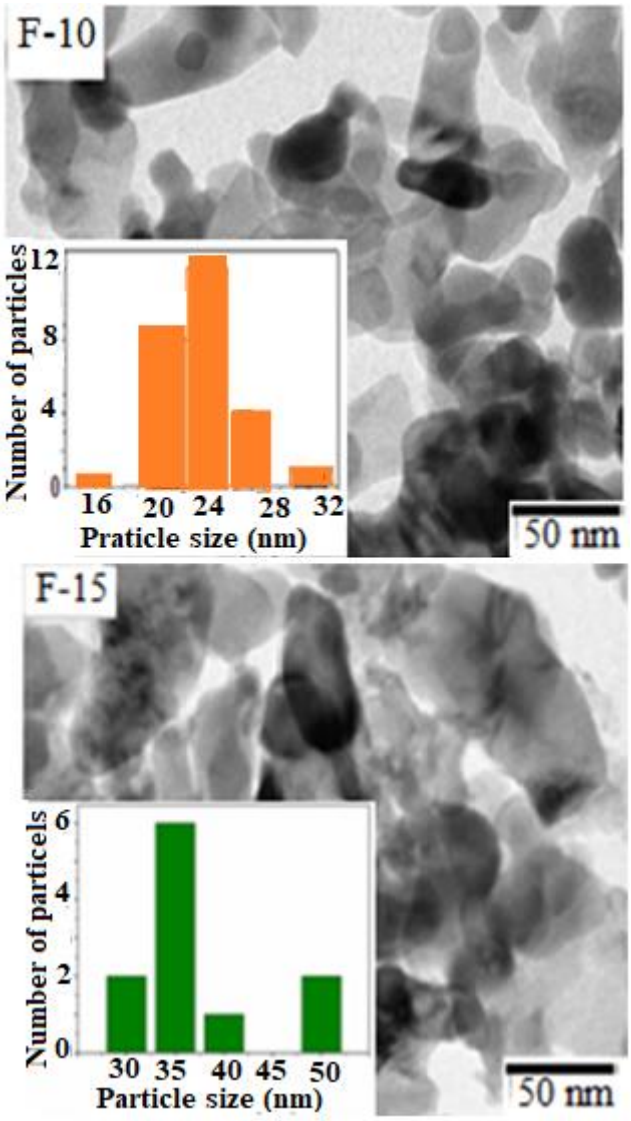

Figure 3. TEM images of F-10 and F-15 samples.

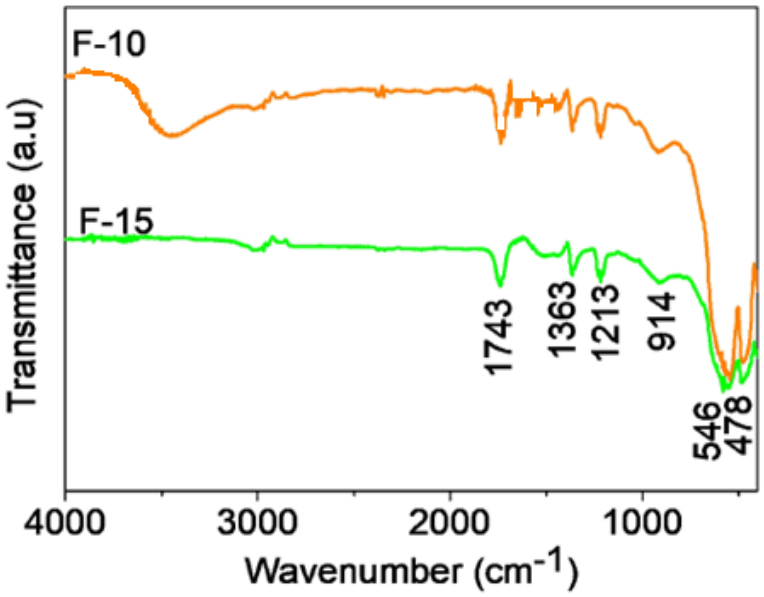

Figure 4. IR spectra of synthesized samples F-10 and F-15

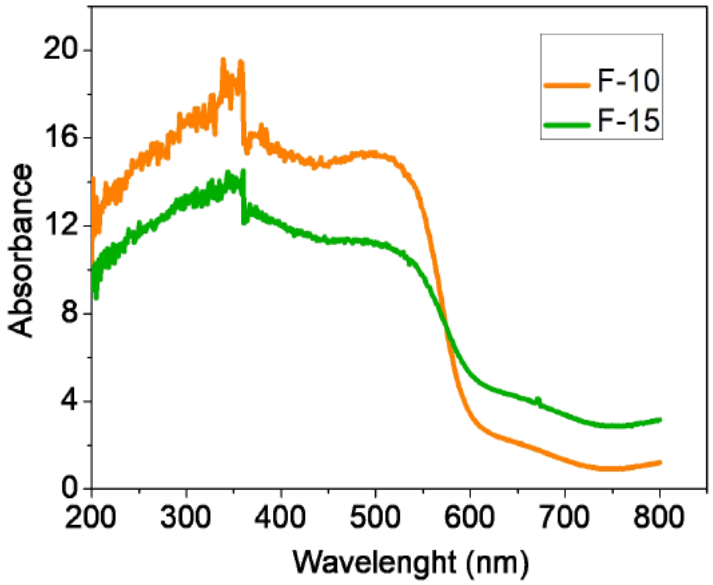

Figure 5. UV –Vis profiles of the α-Fe_2O_3 samples F-10 and F-15

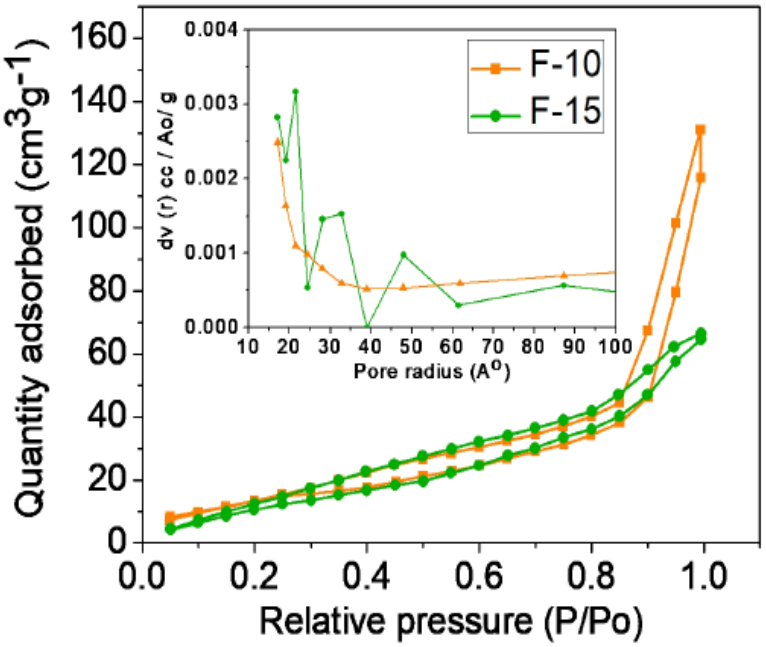

Figure 6. N_2 adsorption desorption isotherm of F-10 and F-15 with inset showing pore size distribution profiles.

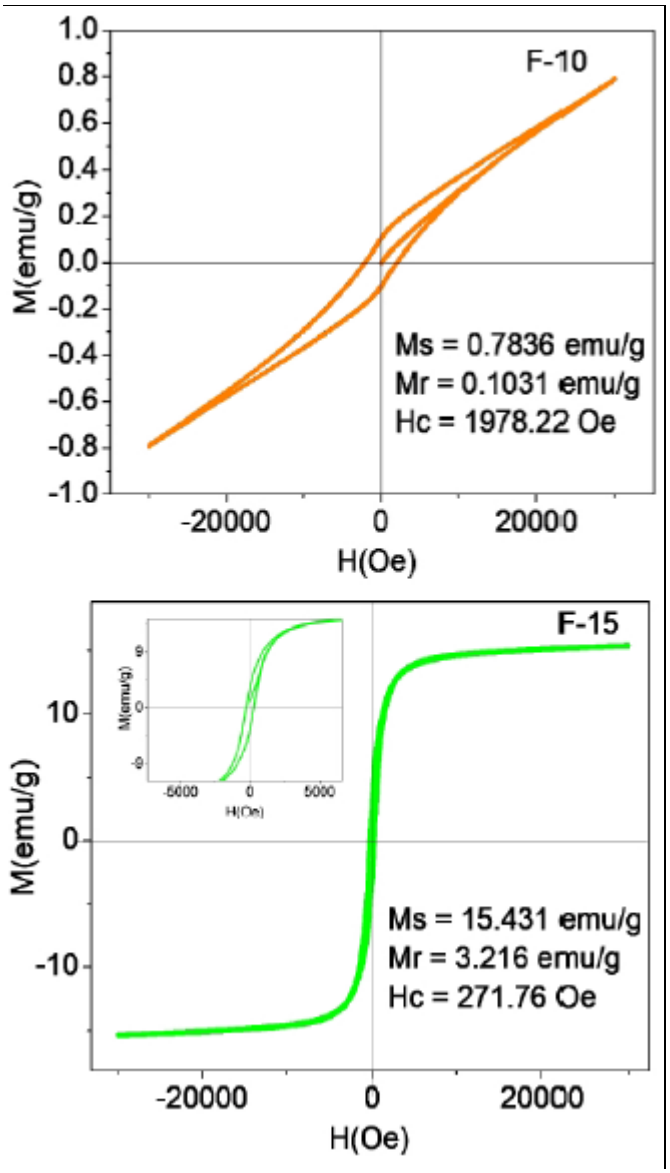

Figure 7. Hysteresis profile for the F-10 and F-15.

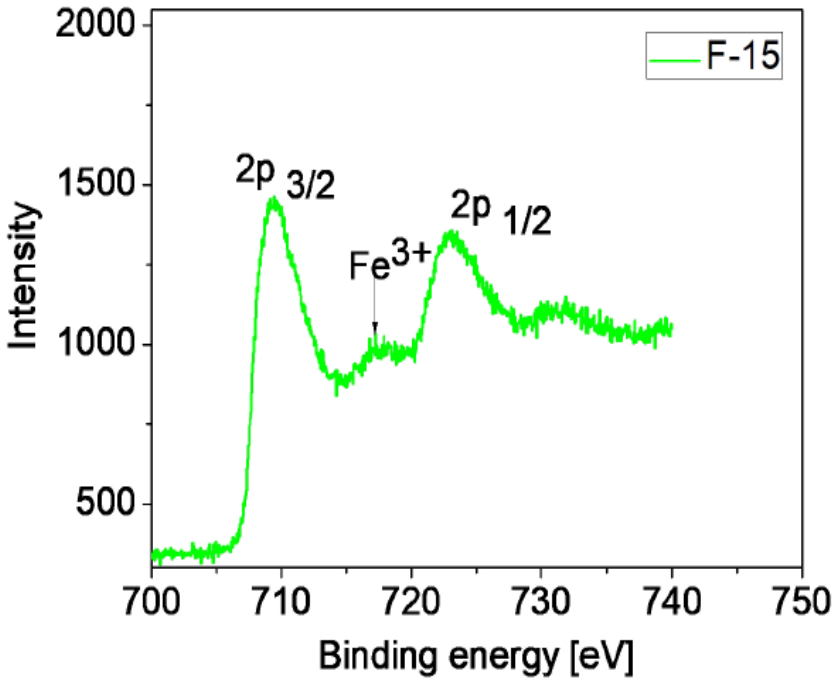

Figure 8. XPS spectra of F-15 sample.

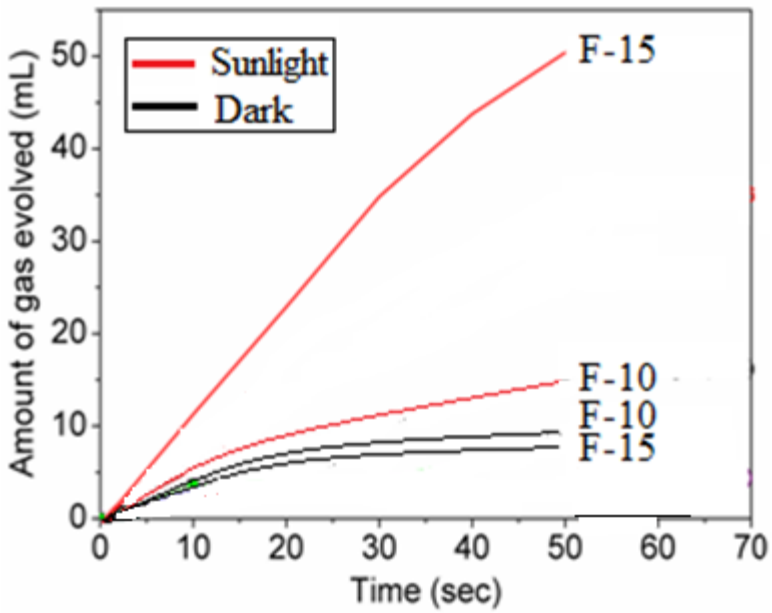

Figure 9 Decomposition of H_2O_2 on the F-10 andF-15 catalysts with exposure to sunlight or without exposure to sunlight (dark).